Toward Noisy One-Bit Diffraction Tomography

Pengwen Chen [1] and Albert Fannjiang[2]

[1]Applied Mathematics, National Chung Hsing University, Taichung, 402, Taiwan
[2]Department of Mathematics, University of California, Davis, CA 95616, USA

October 13, 2023

Abstract

A reconstruction scheme based on one-bit intensity-only measurement with a coded aperture is shown to possess remarkable noise robustness in 3D diffraction tomography.

1 Introduction

Diffraction tomography is a distinct variant of tomographic imaging techniques that predominantly employs wave diffraction, as opposed to absorption, as the fundamental mode of object-wave interaction. At the heart of diffraction tomography is the goal to uncover the object's interior structure by acquiring scattered wavefield data from various orientations around the object. Unlike absorption-based methods, in this technique, both the phase and amplitude of the diffracted waves provide vital information about the object's internal structure. This technique is particularly useful in areas such as non-destructive testing, biomedical imaging, geophysics, and more, where the wavelength of the probing wave is on par with the dimensions of the object or inhomogeneity in the medium, resulting in diffraction phenomena.

In a traditional diffraction tomography setup, the complex-valued scattered wavefield, containing both amplitude and phase information, would be measured. However, in the case of intensity-only measurement, only the magnitude of the scattered wavefield is measured. This approach simplifies the detection process as it circumvents the challenge of phase measurement, which often requires complex and precise instruments like interferometers.

In the context of diffraction tomography with threshold-crossing intensity-only measurements, we are dealing with a binary representation of the diffracted wave's intensity, which inherently simplifies the data acquisition and processing stages. The twist in this technique is that instead of recording the precise intensity of the scattered waves, the measurements are further simplified to a binary or 1-bit representation through threshold crossing. A certain threshold intensity level is predefined, and the sensor only records whether the intensity of the scattered wave is above or below this threshold. In other words, we record a "1" when the intensity is above the threshold and a "0" when it's below.

This binary data is simpler to collect and process, and it's less sensitive to noise compared to full-waveform data. However, such thresholding inevitably leads to a loss of information about the object, making the subsequent image reconstruction process more challenging. Consequently, the choice to use 1-bit intensity-only measurements must carefully balance the benefits of reduced data requirements and increased simplicity against the loss of potentially valuable phase information.

The image reconstruction process typically involves solving an inverse problem to recover the object's properties from the binary data. Given the nature of the data, this is usually a non-linear and ill-posed problem. Reconstruction methods might involve iterative techniques or machine learning-based approaches trained specifically for this kind of data.

The design of the threshold for 1-bit measurement is a vital consideration in diffraction tomography with 1-bit intensity data. This threshold is instrumental in differentiating the measured intensities into categories: either above or below the threshold. Identifying the optimal threshold is a non-trivial task that involves thorough consideration of the specific application, noise levels, and object characteristics. The selected threshold directly influences the quality of the final image reconstruction, underscoring the

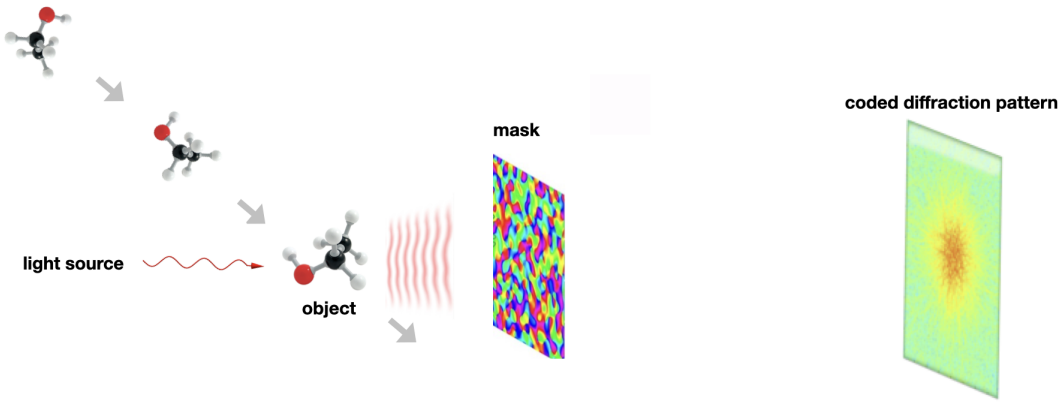

Figure 1: Diffraction patterns in various orientations measured with a random mask

importance of careful threshold design. Traditional reconstruction techniques, like filtered backprojection or Radon inversion methods, which are suitable for high-precision measurements, may not work effectively for 1-bit intensity-only measurements due to their binary nature and the absence of phase information.

Before ending our introduction, let us briefly recall some key advances and insights in the related area of signal reconstruction of two-dimensional complex band-limited signals from *threshold crossings in the real and imaginary parts*.

On one hand, at the Nyquist rate, a band-limited signals can be reconstructed from samples of infinite precision. On the other hand, a band-limited signal whose entire extension is irreducible is uniquely determined, up to some constant factor, by the sign information (real zero-crossings) of its real and imaginary parts, requiring essentially 2-bit information of the samples. While the former case has a robust performance with respect to sample imprecision, the latter case requires, in theory and practice, extreme accuracy in identifying zero crossings [4, 8, 10]. Furthermore, the choice of the threshold level can significantly impact the quality of the reconstruction, making it a crucial factor to consider in the design of such systems.

In closing this section, our tentative goal in this paper is to explore the extreme case of reconstructing 3D objects by tomographic phase retrieval from 1-bit threshold crossings in projected diffraction patterns sampled at the Nyquist rate. In particular, we want to demonstrate the noise reduction effect with 1-bit intensity-only measurement with a coded aperture.

As such, the task is, however, essentially untenable in view of the aforementioned instability in reconstruction from *approximate* information of zero-crossings. One promising approach is to use a randomly coded aperture in the measurement of diffraction patterns [5], resulting in coded diffraction patterns whose thresholding crossings (with a properly chosen threshold) contain substantial amount of information about the underlying object. The idea is motived by a theorem about random matrices proved in [3], which is stated below after setting up some notation.

2 Random-matrix-theoretical basis

Consider the nonlinear signal model: $b = |\mathcal{A}f_*|$, where $\mathcal{A} \in \mathbb{C}^{M\times N}$ is the measurement matrix and $|\cdot|$ denotes entrywise modulus. We select a threshold to separate the "weak" signals, due to destructive interference, from the "strong" signals, due to constructive interference, as follows. Let $I \subset \{1, \cdots, N\}$ be the support set of the weak signals (to be determined) and I_c its complement such that $b[i] \le b[j]$ for all $i \in I, j \in I_c$. Denote the sub-row matrices with row indices in I and I_c by $\mathcal{A}_I$ and $\mathcal{A}_{I_c}$, respectively.

The significance of the weak signal support I lies in the fact that I constains the best loci to "linearize" the problem since b_I is "small". This motivates the least squares problem:

$$\min \left\{ \|\mathcal{A}_I f\|^2 : f \in \mathbb{C}^N, \|f\| = \|f_*\| \right\}. \tag{1}$$

A slightly simplified version of the theorem in [3] is the following.

Theorem 1. *[3] Let $\mathcal{A}$ be a $M \times N$ i.i.d. complex Gaussian matrix and $f_{\min}$ a minimizer of (1). Suppose*

$$N < |I| \ll M \ll |I|^2. \tag{2}$$

Then with an overwhelming probability, the relative error bound

$$\|f_* f_*^* - f_{\min} f_{\min}^*\|_{\mathrm{F}} / \|f_*\|^2 \quad \leq \quad c_0 \sqrt{|I|/M} \ll 1 \tag{3}$$

holds for some constant c_0, where $\|\cdot\|_{\mathrm{F}}$ denotes the Frobenius norm.

In practice, it is convenient to consider the following surrogate:

$$f_{\max} \in \arg\max \left\{ \|\mathcal{A}_{I_c} f\|^2 : f \in \mathcal{X}, \|f\| = \|f_*\| \right\} \tag{4}$$

which approximates $f_{\min}$ as $M \to \infty$. This can be seen as follows.

As $M \to \infty$, the column vectors of $\mathcal{A} = [a_{ij}]$ have nearly the same norm $M^{1/2}$ (assume unit variance for each entry a_{ij}) and are nearly mutually orthogonal in the sense that

$$M^{-1} \sum_{i=1}^{M} \bar{a}_{ij} a_{ik} \sim M^{-1/2} \to 0, \quad j \neq k.$$

In other words, we can think of $M^{-1/2}\mathcal{A}$ as an isometry when M is much larger than N. By the isometry property

$$\|f\|^2 = M^{-1} \|\mathcal{A}_I f\|^2 + M^{-1} \|\mathcal{A}_{I_c} f\|^2, \tag{5}$$

minimizing $\|\mathcal{A}_I f\|^2$ is equivalent to maximizing $\|\mathcal{A}_{I_c} f\|^2$ over $\{f : \|f\| = \|f_*\|\}$.

Problem (4) can be solved conveniently by the projected power method as in Algorithm 1.

Algorithm 1: The Projected Power Method

Input: The indicator vector ω for I_c;
Random initialization: $f^{(1)} = f_{\mathrm{rand}}$
Loop:
for $k = 1 : k_{\max} - 1$ **do**
  $g^{(k)} \leftarrow \mathcal{A}^*(\omega \odot \mathcal{A} f^{(k)})$;
  $f^{(k+1)} \leftarrow \mathcal{P}_{\mathcal{X}} g^{(k)} / \|\mathcal{P}_{\mathcal{X}} g^{(k)}\|$ where $\mathcal{P}_{\mathcal{X}}$ is the the object domain projection.
end
Output: $f^{k_{\max}}$.

The presence of $\mathcal{P}_{\mathcal{X}}$ in Algorithm 1 is due to anticipation of object prior information such as support constraint resulting from zero-padding in tomography (see Section 3).

Given the randomness assumption and the asymptotic nature of the reconstruction accuracy guaranteed by of Theorem 1, it is expected that 1-bit phase retrieval with coded diffraction patterns is similarly asymptotic in the sense that the quality gradually increases as the numbers of diffraction patterns and random masks increase.

A slight drawback with the approach (4) is that $\|f_*\|$ is not known *a priori*. An alternative formulation can be developed for the transform domain as follows. The projected power iteration can be expressed as

$$z^{(k+1)} \quad = \quad \omega \odot \mathcal{P}(\omega \odot z^{(k)}) \tag{6}$$

where $\mathcal{P} = \mathcal{A}\mathcal{A}^\dagger$ is the orthogonal projection on the space $\mathcal{A}\mathcal{X}$.

A limit point z_* of $\{z^{(k)}\}_k$ solves the following optimization problem

$$z_* \in \arg \max_{\|z\| = \|b\|} \|\mathcal{P}(\omega \odot z)\|^2 = \arg \max_{\|z\| = \|b\|} \langle z, P_\omega z \rangle, \ \mathcal{P}_\omega = \mathrm{diag}(\omega) \mathcal{P} \mathrm{diag}(\omega). \tag{7}$$

and the object can be estimated by $\mathcal{A}^\dagger z_*$.

In the appendices we describe an efficient algorithm for computing the pseudo-inverse $\mathcal{A}^\dagger$ in the context of diffraction tomography.

2.1 Noise robustness

Let us consider some heuristic for de-noising effect of the 1-bit intensity-only scheme.

Conceptually the noise level is measured by the noise-to-signal ratio (NSR)

$$\text{NSR} := \frac{\text{Total \# average noise photons}}{\text{Total \# signal photons}}, \tag{8}$$

the reciprocal of the signal-to-noise ratio (SNR). At any given noise level, the I/I_c-membership of the indices near the threshold are least robust to noise while the membership of the extreme (very strong or very weak) indices are most robust to noise.

We want to show that these robust indices and the corresponding row vectors also play the strongest role in the synthesis of $f_{\max}$ and f_*.

Let a_j^T denote the j-th row vector of $\mathcal{A}$. We can write

$$\mathcal{A}^*(\omega \odot \mathcal{A}) = \sum_{j \in I_c} \overline{a_j} a_j^T, \tag{9}$$

the sum of rank-one projections restricted to I_c. Here and below, the over-line notation denotes the complex conjugation.

By Theorem 1, the leading eigenvector $f_{\max}$ of the Gram matrix (9) approximates the true object f_*, so we have

$$f_* \sim \sum_{j \in I_c} \overline{a_j} (a_j^T f_*) \tag{10}$$

which can be interpreted as a linear decomposition of f_* into its features $\{\overline{a_j} : j \in I_c\}$ with coefficients $a_j^T f_*$. As expected, the larger the **noiseless** data $|a_j^T f_*|$, the more significant the corresponding feature $\overline{a_j}$ in the synthesis of f_*.

Thereby lies the de-noising mechanism of the one-bit scheme. Our numerical simulations below provide ample evidence for the plausibility of this idea.

3 Discrete tomography

In a diffraction-limited imaging system such as X-ray crystallography the resolution length is roughly $\lambda/2$. The grid system with spacing $\lambda/2$ gives a reasonable representation of the object continuum without resulting in unnecessary complexity.

Let $[\![k, l]\!]$ denote the integers between and including the integers k and l. Let O_n denote the class of discrete complex-valued objects

$$O_n := \{f : f(i,j,k) \in \mathbb{C}, (i,j,k) \in \mathbb{Z}_n^3; f(i,j,k) = 0, (i,j,k) \notin \mathbb{Z}_n^3\} \tag{11}$$

where

$$\mathbb{Z}_n \quad = \quad \begin{cases} [\![-n/2, n/2-1]\!] & \text{if } n \text{ is an even integer;} \\ [\![-(n-1)/2, (n-1)/2]\!] & \text{if } n \text{ is an odd integer.} \end{cases} \tag{12}$$

To fix the idea, we consider the case of odd n in the paper.

Following the framework in [1] we discretize the projection geometry as follows.

We define three families of line segments, the x-lines, y-lines, and z-lines. The x-lines, denoted by $\ell_{(1,\alpha,\beta)}(c_1, c_2)$ with $|\alpha|, |\beta| < 1$, are defined by

$$\ell_{(1,\alpha,\beta)}(c_1, c_2) : \begin{bmatrix} y \\ z \end{bmatrix} = \begin{bmatrix} \alpha x + c_1 \\ \beta x + c_2 \end{bmatrix} \qquad c_1, c_2 \in \mathbb{Z}_{2n-1}, \quad x \in \mathbb{Z}_n \tag{13}$$

To avoid wraparound of x-lines with , we can zero-pad f in a larger lattice $\mathbb{Z}_p^3$ with $p \geq 2n-1$. This is particularly important when it comes to define the ray transform by a line sum (cf. (19)-(21)) since wrap-around is unphysical. To fixed the idea, we define the object space that we shall work with:

$$\mathcal{X} := \{f \in O_n \text{ with the domain restricted to } \mathbb{Z}_{2n-1}^3\}. \tag{14}$$

Similarly, a y-line and a z-line are defined as

$$\ell_{(\alpha,1,\beta)}(c_1,c_2):\begin{bmatrix}x\\z\end{bmatrix}=\begin{bmatrix}\alpha y+c_1\\ \beta y+c_2\end{bmatrix}\qquad c_1,c_2\in\mathbb{Z}_{2n-1},\quad y\in\mathbb{Z}_n, \tag{15}$$

$$\ell_{(\alpha,\beta,1)}(c_1,c_2):\begin{bmatrix}x\\y\end{bmatrix}=\begin{bmatrix}\alpha z+c_1\\ \beta z+c_2\end{bmatrix}\qquad c_1,c_2\in\mathbb{Z}_{2n-1},\quad z\in\mathbb{Z}_n, \tag{16}$$

with $|\alpha|,|\beta|<1$.

Let $\widetilde{f}$ be the continuous interpolation of f given by

$$\widetilde{f}(x,y,z) \;=\; \sum_{i\in\mathbb{Z}_n}\sum_{j\in\mathbb{Z}_n}\sum_{k\in\mathbb{Z}_n} f(i,j,k)D_p(x-i)D_p(y-j)D_p(z-k),\quad x,y,z,\in\mathbb{R}, \tag{17}$$

where D_p is the p-periodic Dirichlet kernel given by

$$D_p(t)=\frac{1}{p}\sum_{l\in\mathbb{Z}_p} e^{\mathrm{i}2\pi lt/p} \;=\; \begin{cases}1, & t=mp,\quad m\in\mathbb{Z}\\ \frac{\sin(\pi t)}{p\sin(\pi t/p)}, & \text{else.}\end{cases} \tag{18}$$

In particular, $[D_p(i-j)]_{i,j\in\mathbb{Z}_p}$ is the $p\times p$ identity matrix. Because D_p is a continuous p-periodic function, so is $\widetilde{f}$. However, we will only use the restriction of $\widetilde{f}$ to one period cell $[-(p-1)/2,(p-1)/2]^3$ to define the discrete projections and avoid the wraparound effect.

We define the discrete projections as the following line sums

$$f_{(1,\alpha,\beta)}(c_1,c_2) \;=\; \sum_{i\in\mathbb{Z}_n}\widetilde{f}(i,\alpha i+c_1,\beta i+c_2), \tag{19}$$

$$f_{(\alpha,1,\beta)}(c_1,c_2) \;=\; \sum_{j\in\mathbb{Z}_n}\widetilde{f}(\alpha j+c_1,j,\beta j+c_2) \tag{20}$$

$$f_{(\alpha,\beta,1)}(c_1,c_2) \;=\; \sum_{k\in\mathbb{Z}_n}\widetilde{f}(\alpha k+c_1,\beta k+c_2,k) \tag{21}$$

with $c_1,c_2\in\mathbb{Z}_{2n-1}$.

The 3D discrete Fourier transform $\mathcal{F}f$ of the object $f\in\mathcal{X}$, is given by

$$\mathcal{F}f(\xi,\eta,\zeta) \;=\; p^{-3/2}\sum_{i,j,k} f(i,j,k)e^{-\mathrm{i}2\pi(\xi i+\eta j+\zeta k)/p} \tag{22}$$

where the range of the Fourier variables ξ,η,ζ can be extended from the discrete interval $\mathbb{Z}_p$ to the continuum $[-(p-1)/2,(p-1)/2]$. Note that by definition, $\widehat{f}$ is a p-periodic band-limited function. When there is no risk of confusion, we shall denote the *full* DFT for 1D and 2D functions g by $\mathcal{F}g$ and use the shorthand notation $\widehat{g}=\mathcal{F}g$.

For z-lines, let $\mathbf{t}=(\mathbf{t}',1)$ with $\mathbf{t}'=(\alpha,\beta)$ denote the direction vectors. Let $f_{\mathbf{t}}$ denote the discrete ray transform

$$f_{\mathbf{t}}(c):=\sum_{j\in\mathbb{Z}_n} f\left(\mathbf{t}'j+c,j_3\right),\quad \mathbf{c}=(c_1,c_2)\in\mathbb{Z}_p^2. \tag{23}$$

Let $\mathcal{T}$ denote the set of directions $\mathbf{t}$ employed in the 3D diffraction measurement with a coded aperture (Figure 1). To fix the idea, let $p=2n-1$ in (18).

Let μ be the mask function and $f_{\mathbf{t}}$ the object projection in the direction $\mathbf{t}$. The Fourier transform of the masked exit wave in Figure 1 is given by

$$\mathcal{F}(f_{\mathbf{t}}\odot\mu) \;=\; p^{-1}\widehat{f}_{\mathbf{t}}*\widehat{\mu}(\mathbf{n}):=p^{-1}\sum_{\mathbf{n}'\in\mathbb{Z}_p^2}\widehat{f}_{\mathbf{t}}(\mathbf{n}')\widehat{\mu}(\mathbf{n}-\mathbf{n}'). \tag{24}$$

We decompose the measurement process into two steps:

$$\mathcal{X}\xrightarrow{\mathcal{R}}\mathcal{X}_{\mathcal{T}}:=\{(f_{\mathbf{t}})_{\mathbf{t}\in\mathcal{T}}:f\in\mathcal{X}\}\xrightarrow{\mathcal{Q}}\{(\widehat{f}_{\mathbf{t}}*\widehat{\mu})_{\mathbf{t}\in\mathcal{T}}:f\in\mathcal{X}\} \tag{25}$$

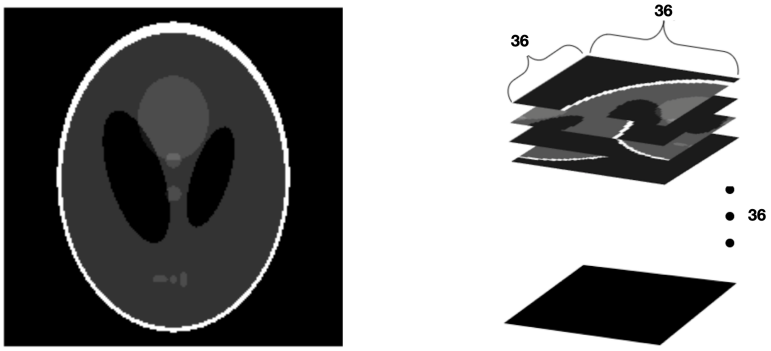

(a) 2D image (b) 3D representation

Figure 2: 216×216 image $\Longrightarrow$ $36 \times 36 \times 36$ object.

with the "collective" ray-transform $\mathcal{R}$ and the masked Fourier transform $\mathcal{Q}$. Now we can write the noiseless signal model as $b = |\mathcal{A}f|$, with the measurement matrix $\mathcal{A} := \mathcal{Q}\mathcal{R}$. The object domain projection $\mathcal{P}_{\mathcal{X}}$ in Algorithm 1 is now represented in the transform domain as

$$\mathcal{P} = \mathcal{Q}\mathcal{R}(\mathcal{Q}\mathcal{R})^{\dagger} = \mathcal{Q}\mathcal{R}(\mathcal{R}^*\mathcal{R})^{-1}\mathcal{R}^*\mathcal{Q}^*. \tag{26}$$

For simplicity, let us assume that μ is a phase mask, i.e. $\mu = \exp[\mathrm{i}\phi], \phi \in \mathbb{R}$. Then for each $\mathbf{t}$ the mapping (24) defined for $f_{\mathbf{t}}$ is an isometry, modulo a scale factor, while the tomographic mapping $\mathcal{A}$ defined for the 3D object f is not. Therefore, the threshold for one-bit measurement is to be set separately for each coded diffraction pattern (see below). Surprisingly, such a procedure possesses the noise robustness discussed in Section 2.1.

4 Numerical simulations

In our simulations, we take the mask phase ϕ to be an independent uniform random variable over $[0, 2\pi)$ for each pixel.

We construct the real-valued 3D object from the 216×216 phantom (Fig. 2 (a)) by partitioning the phantom into 36 pieces, each of which is 36×36 and stacking them into a $36 \times 36 \times 36$ cube (Fig. 2(b)). This is partly motivated by the observation that in highly noisy reconstruction the traditional error metric (such as relative error) is not as meaningful as the "eye-ball" metric, which can be readily facilitated by using a 3D object constructed from a 2D image.

We also consider the complex-valued version of the 3D phantom by randomly modulated the phase of each voxel and call it 3D randomly phased phantom (RPP). The number of unknowns in RPP is twice of that in phantom.

In addition to the "eye-ball" metric, we also show the absolute correlation between f_* and reconstruction f given by

$$R(f, f_*) := \frac{|f^* f_*|}{\|f\|\|f_*\|}.$$

In our numerical results below, the absolute correlation largely corroborates with the visual quality of the reconstruction.

We use the reconstruction scheme (6) with the threshold for each coded diffraction pattern given by the median value (the median rule), i.e. $|I_j| = p^2/2, j = 1, \cdots, m$ where I_j is the index set of weak signals in the j-th coded diffraction pattern. We set the threshold for each coded diffraction pattern because the nature of diffraction pattern may be highly sensitive to the direction of illumination. Our choice of threshold (the median rule) is consistent with the condition (2). For other convenient rules for the threshold see [3].

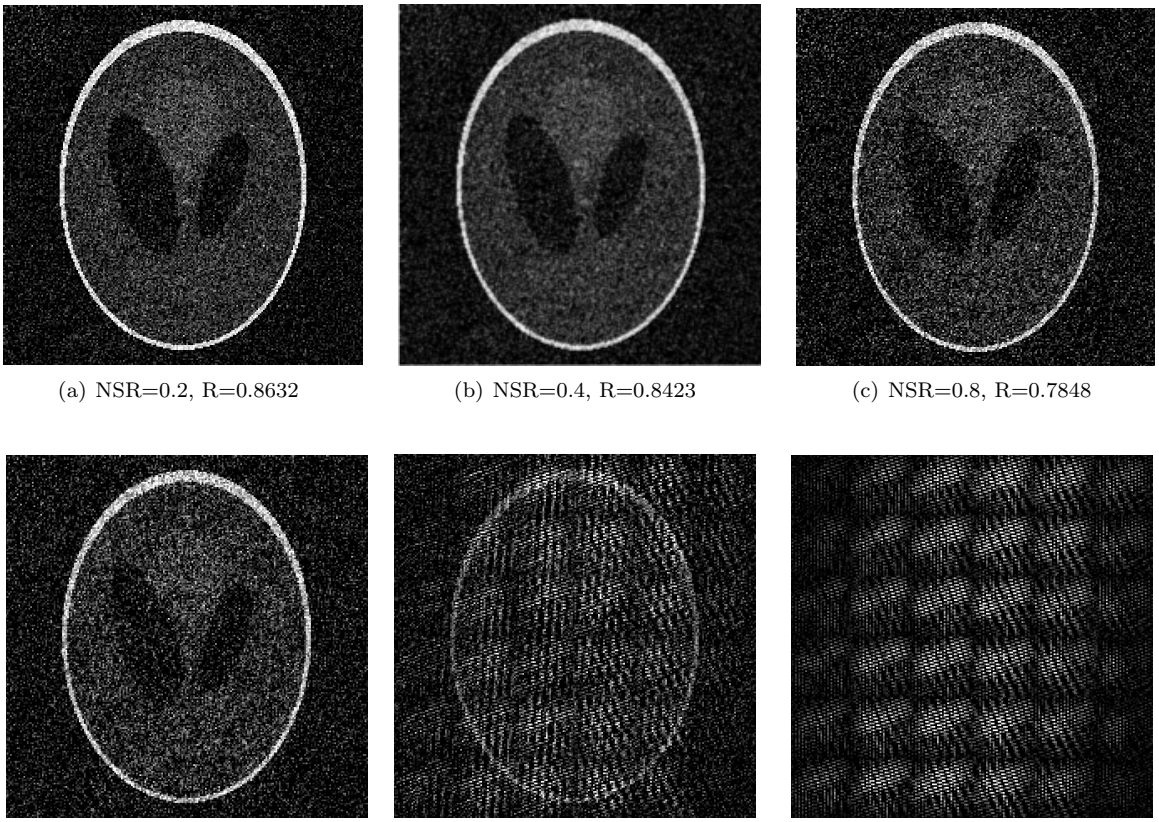

(a) NSR=0.2, R=0.8632 (b) NSR=0.4, R=0.8423 (c) NSR=0.8, R=0.7848

(d) NSR=1.25, R=0.7587 (e) NSR=2.5, R=0.4989 (f) NSR=5.0, R=0.3419

Figure 3: 3D phantom reconstruction with Poisson noises.

To avoid the missing cone problem in tomography, we consider $m = 3\rho n$ evenly distributed random directions

$$\begin{aligned} \mathcal{T} &= \{\mathbf{t}_i = (1, \alpha_i, \beta_i)\}_{i=1}^{\rho n} \cup \{\mathbf{t}_i = (\alpha_i, 1, \beta_i)\}_{i=1+\rho n}^{2\rho n} \cup \{\mathbf{t}_i = (\alpha_i, \beta_i, 1)\}_{i=2\rho n+1}^{3\rho n} \\ &\quad \text{with } \alpha_i, \beta_i, i = 1, \cdots, 3n, \text{ randomly chosen from } (-1, 1) \end{aligned} \tag{27}$$

with the parameter $\rho \in \mathbb{N}$. According to [6, 7], a non-degenerate set of $n + 1$ directions suffice for uniqueness, modulo phase factor, for diffraction tomography with noiseless data. For 1-bit diffraction tomography with highly noisy data, however, one should deploy a far larger set of directions to obtain any reasonable results.

4.1 Noise-to-signal ratio (NSR)

Photon noise, also called shot noise, is due to the statistical nature of photon emission and detection. When light passes through a phase mask and creates a diffraction pattern, the photon noise in that pattern is fundamentally dictated by the number of photons detected at each point in the pattern.

Photon noise is commonly described by the Poisson distribution such that the noisy intensity data vector $\widetilde{b^2}$ has as the noise components the independent Poisson random variables with the means equal to the noiseless components. To introduce the Poisson noise into our mathematical set-up, let $b^2 = |\mathcal{A}f_*|^2$ as before but consider sb^2 to be the noiseless intensity data with an adjustable scale factor $s > 0$ representing the overall strength of object-radiation interaction.

Denote the intensity fluctuation by $z = (z_j)$. The (deterministic) noise photon count is $\sum_j |z_j|$ and

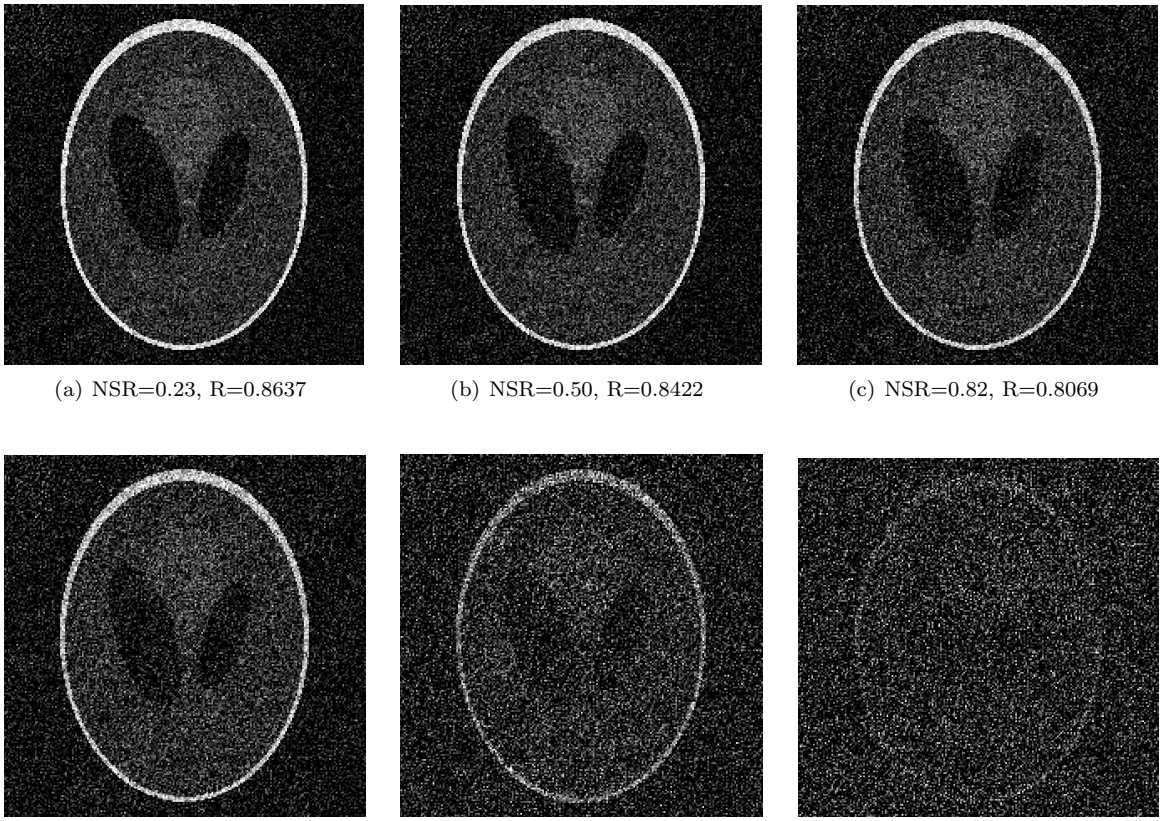

(a) NSR=0.23, R=0.8637 (b) NSR=0.50, R=0.8422 (c) NSR=0.82, R=0.8069

(d) NSR=1.21, R=0.7622 (e) NSR=3.56, R=0.5745 (f) NSR=12.54, R=0.3815

Figure 4: 3D phantom reconstruction with Gaussian noises with $\sigma = 0.4, 0.8, 1.2$ (top) and $\sigma = 1.6$, 3.2, 6.4 (bottom).

the total average noise photon count is given by

$$\sum_j \mathbb{E}|z_j| \quad \text{or more conveniently} \quad \sum_j \sqrt{\mathbb{E}|z_j|^2} = \left\| \sqrt{\mathbb{E}|z_j|^2} \right\|_1 \tag{28}$$

where $\|\cdot\|_1$ denotes the L1-norm of the vector. In the case of Poisson noise, $z = \widetilde{b}^2 - sb^2$ and hence the total number of average noise photons is given by $\left\| \sqrt{\mathbb{E}(\widetilde{b}^2 - sb^2)^2} \right\|_1$. In other words, NSR as given in (8) can be precisely defined as

$$\text{NSR} \quad := \quad \frac{\left\| \sqrt{\mathbb{E}(\widetilde{b}^2 - sb^2)^2} \right\|_1}{s\|b^2\|_1}. \tag{29}$$

By a straightforward calculation with the Poisson distribution, we have

$$\text{NSR} \quad = \quad \frac{\|b\|_1}{\sqrt{s}\|b^2\|_1}. \tag{30}$$

In the case of the Gaussian additive noise, the noisy data is defined as

$$\widetilde{b} := |\mathcal{A}f_* + \nu|$$

where ν are the i.i.d. circularly symmetric complex Gaussian random variables with a given variance σ^2. The NSR is given by

$$\text{NSR} \quad := \quad \frac{\left\| \sqrt{\mathbb{E}(\widetilde{b}^2 - b^2)^2} \right\|_1}{\|b^2\|_1}. \tag{31}$$

By a straightforward calculation with independent circularly symmetric Gaussian random variables, we have

$$\begin{aligned} \mathbb{E}(\widetilde{b}^2 - b^2)^2 &= \mathbb{E}|\nu|^4 + \mathbb{E}(\mathcal{A}f_* \odot \overline{\nu} + \overline{\mathcal{A}f_*} \odot \nu)^2 \\ &= \mathbb{E}|\nu|^4 + 2b^2 \odot \mathbb{E}|\nu|^2. \end{aligned} \tag{32}$$

By definition, $\mathbb{E}\Re(\nu)^2 = \mathbb{E}\Im(\nu)^2 = \sigma^2/2$ and

$$\begin{aligned} \mathbb{E}|\nu|^4 &= \mathbb{E}(\Re(\nu)^2 + \Im(\nu)^2)^2 \\ &= \mathbb{E}\Re(\nu)^4 + \mathbb{E}\Im(\nu)^4 + 2\mathbb{E}(\Re(\nu)^2 \odot \Im(\nu)^2) \\ &= 3(\sigma^2/2)^2 + 3(\sigma^2/2)^2 + 2(\sigma^2/2)^2 \\ &= 2\sigma^4. \end{aligned} \tag{33}$$

Hence

$$\text{NSR} \quad = \quad \sqrt{2}\sigma \frac{\|\sqrt{\sigma^2 + b^2}\|_1}{\|b^2\|_1} \tag{34}$$

4.2 Numerical results

Reconstruction of 3D phantom with $\rho = 2$ in (27) are carried out by the projected power method (6) and shown, respectively, in Fig. 3 and 4 for the Poisson and Gaussian noise, respectively, at various noise levels. In both cases, the quality of reconstruction is reasonably good up to NSR ≈ 1.2 in terms of the visual quality of flattened reconstruction. Beyond this noise level, the quality of reconstruction deteriorates differently for the two noise models, with the Poisson noise model less gracefully.

For 3D RPP, however, $\mathcal{T}$ with $\rho = 2$ results in poor reconstruction regardless of the noise level. With the number of directions increasing to $\rho = 4$ in (27), the performance (Figure 5) is much improved and even superior to those for 3D phantom with $\rho = 2$. The high level of correlation (> 0.96) for NSR up to 0.6 is quite remarkable.

(a) NSR=0, R=0.9789 (b) NSR=0.6, R=0.9632 (c) NSR=1.25, R=0.8331

Figure 5: The magnitude of 3D RPP reconstruction with the Poisson noise.

5 Conclusion

In the present note, we demonstrate the de-noising effect of the 1-bit scheme with coded aperture for diffraction tomography. The same approach can be applied to ptychography when the adjacent coded apertures have sufficient overlaps.

Redundancy in measurement is the key for overcoming noise effects and can be gauged by the oversampling ratio generally defined as

$$\frac{\text{Total \# measurement data}}{\text{\# (real) unknown variables}}.$$

In the simulations for 3D phantom, there are $6n$ diffraction patterns each of which is a $p \times p$ array with $p = 2n - 1$. Since the number of unknown variables is n^3, the overall oversampling ratio is

$$\frac{6n(2n-1)^2}{n^3} \approx 24.$$

In the simulations for 3D RPP, both the number of unknowns and the number of directions double, resulting in the same overall oversampling ratio.

Part of the redundancy is due to the cubic nature of the object support $\mathbb{Z}_n^3$. On the other hand, the same measurement scheme should suffice for 3D objects supported within the sphere of radius $\sqrt{3}n/2$ which circumscribes $\mathbb{Z}_n^3$ and contains roughly $\sqrt{3}\pi n^3/2 \approx 2.7n^3$ lattice points, resulting in a lower oversampling ratio $24/2.7 \approx 8.8$.

A Pseudo-inverse of $\mathcal{A}$

We adopt the following notation: $\mathcal{F}_i, i = 1, 2, 3$, denotes the 1D DFT in the ith variable over $\mathbb{Z}_p$; $\mathcal{F}_{ij}, i, j = 1, 2, 3$, denotes the 2D DFT in the i- and j-th variables over $\mathbb{Z}_p^2$; $\mathcal{F}$ denotes the 3D DFT over $\mathbb{Z}_p^3$.

Note that $A^\dagger = \mathcal{R}^\dagger \mathcal{Q}^\dagger = p^{-1}\mathcal{R}^\dagger \mathcal{Q}^*$ which numerically hinges on efficient implementation of $\mathcal{R}^\dagger$.

First consider the case of projections along z-lines only. We have

$$\begin{aligned} f_{\mathbf{t}}(\mathbf{c}) &= \sum_{j \in \mathbb{Z}_n} f\left(\mathbf{t}' j + \mathbf{c}, j\right) \\ &= p^{-2} \sum_{\mathbf{k}} \sum_{j} \sum_{\mathbf{j}} f(\mathbf{j}, j) e^{\mathrm{i}2\pi(\mathbf{t}' j + \mathbf{c} - \mathbf{j})\cdot \mathbf{k}/p} \\ &= p^{-2} \sum_{\mathbf{k}} e^{\mathrm{i}2\pi \mathbf{k}\cdot\mathbf{c}/p} \sum_{j} e^{\mathrm{i}2\pi j \mathbf{t}'\cdot\mathbf{k}/p} \sum_{\mathbf{j}} f(\mathbf{j}, j) e^{-2\pi \mathbf{k}\cdot\mathbf{j}/p} \\ &= p^{-1} \sum_{\mathbf{k}} e^{\mathrm{i}2\pi \mathbf{k}\cdot\mathbf{c}/p} \sum_{j} e^{\mathrm{i}2\pi j \mathbf{t}'\cdot\mathbf{k}/p} \mathcal{F}_{12} f(\mathbf{k}, j). \end{aligned} \tag{35}$$

For each $g = (g_j) \in \mathbb{C}^p$, let Φg be the quasi-periodic function given by

$$\Phi g(\zeta) = \sum_{j \in \mathbb{Z}^p} e^{\mathrm{i}2\pi j\zeta/p} g_j, \quad g = (g_j) \in \mathbb{C}^p. \tag{36}$$

For given $\mathbf{k}$ and $\mathcal{T} = \{\mathbf{t}_l = (\mathbf{t}'_l, 1) : l = 1, ..., m\}$ define the matrix Ψ by

$$\Psi g = \Big(\Phi g(\mathbf{t}'_l \cdot \mathbf{k})\Big)_{l=1}^m, \quad g = (g_j) \in \mathbb{C}^p \tag{37}$$

whose adjoint is then given by

$$\Psi^* h \quad = \quad \left(\sum_{l=1}^m e^{-\mathrm{i}2\pi j \mathbf{t}'_l \cdot \mathbf{k}/p} h_l\right)_{j \in \mathbb{Z}_p}, \quad h := (h_l) \in \mathbb{C}^m. \tag{38}$$

By (35) $\mathcal{R}$ acting on $\mathcal{X}$ can be decomposed as we have

$$\mathcal{R} = \mathcal{F}_{12}^* \Psi \mathcal{F}_{12}. \tag{39}$$

Since

$$\mathcal{R}^\dagger = \mathcal{F}_{12}^* \Psi^\dagger \mathcal{F}_{12} = \mathcal{F}_{12}^* (\Psi^* \Psi)^{-1} \Psi^* \mathcal{F}_{12}$$

the key to computing $\mathcal{R}^\dagger$ is the inversion of $\Psi^*\Psi$. Indeed, any

$$v := \mathcal{R}^\dagger h, \quad h \in \mathcal{X}_\mathcal{T} := \{(f_\mathbf{t})_{\mathbf{t} \in \mathcal{T}} : f \in \mathcal{X}\} \tag{40}$$

satisfy the normal equation

$$\Psi^* \Psi \mathcal{F}_{12} v \quad = \quad \Psi^* \mathcal{F}_{12} h \tag{41}$$

which is a Toeplitz system in view of the identity

$$\Psi^* \Psi \mathcal{F}_{12} v(\mathbf{k}, j) = \sum_{i \in \mathbb{Z}_p} \sum_{l=1}^m e^{-\mathrm{i}2\pi (j-i) \mathbf{t}'_l \cdot \mathbf{k}/p} \mathcal{F}_{12} v(\mathbf{k}, i). \tag{42}$$

Observe that $\mathcal{F}_{12} v(\cdot, i) = 0$ for all $i \notin \mathbb{Z}_n$ and $i - j \in \mathbb{Z}_p$ for $i, j \in \mathbb{Z}_n$ (with $p = 2n - 1$). Hence $\Psi^*\Psi$ can be implemented as a $p \times p$ circulant matrix when acting on vectors supported on $\mathbb{Z}_n$:

$$\Psi^* \Psi \quad = \quad \left(\sum_{l=1}^m e^{-\mathrm{i}2\pi (j-i) \mathbf{t}'_l \cdot \mathbf{k}/p}\right)_{i,j \in \mathbb{Z}_p}. \tag{43}$$

Consequently, $\Psi^*\Psi$ can be efficiently inverted by diagonalizing with FFT. This fast matrix-vector product motivates the adoption of conjugate gradient (CG) methods for computing $\mathcal{R}^\dagger$.

Let

$$w(\mathbf{k}, k) \quad := \quad \sum_{l=1}^m e^{-\mathrm{i}2\pi k \mathbf{t}'_l \cdot \mathbf{k}/p}, \quad (\mathbf{k}, k) \in \mathbb{Z}_p^3. \tag{44}$$

By (42) and the discrete convolution theorem

$$\Psi^* \Psi \mathcal{F}_{12} v = w *_3 \mathcal{F}_{12} v = \sqrt{p} \mathcal{F}_3^* (\mathcal{F}_3 w \odot \mathcal{F}_3 \mathcal{F}_{12} v) \tag{45}$$

where $*_3$ denotes the discrete convolution over the third variable. Hence

$$\mathcal{F}_{12}^* \Psi^* \Psi \mathcal{F}_{12} v \quad = \quad \sqrt{p} \mathcal{F}^* (\mathcal{F}_3 w \odot \mathcal{F} v). \tag{46}$$

By (41), any $v = \mathcal{R}^\dagger h, h \in \mathcal{X}_\mathcal{T}$ satisfy

$$\sqrt{p} \mathcal{F}^* (\mathcal{F}_3 w \odot \mathcal{F} v) = \mathcal{F}_{12}^* \Psi^* \mathcal{F}_{12} h, \quad v \in \mathcal{X}, \tag{47}$$

which is then solved by CG in the space $\mathcal{X}$.

In summary, we have $A^\dagger = \mathcal{R}^\dagger \mathcal{Q}^\dagger$ where $\mathcal{R}^\dagger$ is obtained by solving eq. (47) with w given by (44).

B $\mathcal{A}^\dagger$ with $x-$, $y-$ and $z-$lines

Let

$$\begin{aligned}
\mathcal{T}_1 &= \{\mathbf{t}_i = (1, \alpha_i, \beta_i) \in \mathbb{R}^3 : i = 1, \cdots, m_1\} && (48)\\
\mathcal{T}_2 &= \{\mathbf{t}_i = (\alpha_i, 1, \beta_i) \in \mathbb{R}^3 : i = m_1 + 1, \cdots, m_1 + m_2\} && (49)\\
\mathcal{T}_3 &= \{\mathbf{t}_i = (\alpha_i, \beta_i, 1) \in \mathbb{R}^3 : i = m_1 + m_2 + 1, \cdots, m_1 + m_2 + m_3\} && (50)
\end{aligned}$$

and $\mathcal{T} = \mathcal{T}_1 \cup \mathcal{T}_2 \cup \mathcal{T}_3$ be the total set of $m = m_1 + m_2 + m_3$ projection directions.

Let $\mathcal{A}_j = \mathcal{Q}_j\mathcal{R}_j$ be the partial measurement matrix and decomposition corresponding to $\mathcal{T}_j, j = 1, 2, 3$. Let $\mathcal{A} = [\mathcal{A}_1^T, \mathcal{A}_2^T, \mathcal{A}_3^T]^T$ be the full measurement matrix which can be decomposed as $\mathcal{A} = \mathcal{Q}\mathcal{R}$ where $\mathcal{Q} = \text{diag}[\mathcal{Q}_1, \mathcal{Q}_2, \mathcal{Q}_3]$ is the collective masked Fourier transform and $\mathcal{R} = [\mathcal{R}_1^T, \mathcal{R}_2^T, \mathcal{R}_3^T]^T$ the collective ray transform.

To compute $\mathcal{A}^\dagger = \mathcal{R}^\dagger\mathcal{Q}^\dagger$ the key is $\mathcal{R}^\dagger$. Since $\mathcal{R}^\dagger = (\mathcal{R}^*\mathcal{R})^{-1}\mathcal{R}^*$, we have

$$\mathcal{R}^\dagger = (\mathcal{R}_1^*\mathcal{R}_1 + \mathcal{R}_2^*\mathcal{R}_2 + \mathcal{R}_3^*\mathcal{R}_3)^{-1}\mathcal{R}^*. \tag{51}$$

Analogous to (39), we have

$$\begin{aligned}
\mathcal{R}_1 &= \mathcal{F}_{23}^*\Psi_1\mathcal{F}_{23}\\
\mathcal{R}_2 &= \mathcal{F}_{13}^*\Psi_2\mathcal{F}_{13}\\
\mathcal{R}_3 &= \mathcal{F}_{12}^*\Psi_3\mathcal{F}_{12}.
\end{aligned}$$

where for any $g = (g_j) \in \mathbb{C}^p$

$$\begin{aligned}
\Psi_1 g &= \Big(\Phi g(\alpha_l k_2 + \beta_l k_3)\Big)_{l=1}^{m_1}\\
\Psi_2 g &= \Big(\Phi g(\alpha_l k_1 + \beta_l k_3)\Big)_{l=m_1+1}^{m_1+m_2}\\
\Psi_3 g &= \Big(\Phi g(\alpha_l k_1 + \beta_l k_2)\Big)_{l=m_1+m_2+1}^{m}
\end{aligned}$$

with the transform Φ defined by (36). Hence by (51), the key to $\mathcal{R}^\dagger$ is to invert the matrix

$$\mathcal{F}_{23}^*\Psi_1^*\Psi_1\mathcal{F}_{23} + \mathcal{F}_{13}^*\Psi_2^*\Psi_2\mathcal{F}_{13} + \mathcal{F}_{12}^*\Psi_3^*\Psi_3\mathcal{F}_{12} \tag{52}$$

or, equivalently, to solve for $v = \mathcal{R}^\dagger h$ from the equation analogous to (47):

$$\sqrt{p}\mathcal{F}^*\Big(u \odot \mathcal{F}v\Big) = \mathcal{R}^*h, \quad u := \sum_{l=1}^{3} \mathcal{F}_l w_l, \tag{53}$$

where $\mathcal{R}^* = [\overline{\mathcal{R}_1}, \overline{\mathcal{R}_2}, \overline{\mathcal{R}_3}]$ (over-line denotes complex conjugation) and

$$\begin{aligned}
w_1(k_1, k_2, k_3) &= \sum_{l=1}^{m_1} e^{-\mathrm{i}2\pi k_1(k_2\alpha_l + k_3\beta_l)/p}, && (54)\\
w_2(k_1, k_2, k_3) &= \sum_{l=m_1+1}^{m_1+m_2} e^{-\mathrm{i}2\pi k_2(k_1\alpha_l + k_3\beta_l)/p}, && (55)\\
w_3(k_1, k_2, k_3) &= \sum_{l=m_1+m_2+1}^{m} e^{-\mathrm{i}2\pi k_3(k_1\alpha_l + k_2\beta_l)/p}. && (56)
\end{aligned}$$

Acknowledgement

The research PC is supported in part by grant 110-2115-M-005-007-MY3 from the Ministry of Science and Technology, Taiwan. The research of AF is supported in part by by the Simons Foundation grant FDN 2019-24 and the US National Science Foundation grant CCF-1934568.

References

[1] A. Averbuch & Y. Shkolnisky, "3D discrete X-ray transform," *Appl. Comput. Harmon. Anal.* **17** (2004) 259-276.

[2] R. H. T. Bates, B. K. Quek, and C. R. Parker, "Some implications of zero sheets for blind deconvolution and phase retrieval," *J. Opt. Soc. Am. A* **7** (1990) 468-479.

[3] P. Chen, A. Fannjiang, G. Liu, "Phase retrieval by linear algebra," *SIAM J. Matrix Anal. Appl.* **38** (2017) 854 - 868.

[4] S. Curtis, S. Shitz and A.V. Oppenheim, "Reconstruction of nonperiodic two-dimensional signals from zero crossings," *IEEE Trans. Acoust. Speech Signal Proc.* **35** (1987) 890-893.

[5] A. Fannjiang, "Absolute uniqueness of phase retrieval with random illumination," *Inverse Problems* **28** (2012) 075008.

[6] A. Fannjiang, "Uniqueness theorems for tomographic phase retrieval with few coded diffraction patterns", *Inverse Problems* **38** (2022) 085008.

[7] A. Fannjiang, " 3D tomographic phase retrieval and unwrapping," arXiv:2208.04798.

[8] J.L.C. Sanz and T. T. Huang, "Image representation by sign information" *IEEE Trans. Pattern Anal. Machine Intel.***11 (7)** (1989) 729-738.

[9] M.S. Scivier and M.A. Fiddy, "Phase ambiguity and the zeros of multidimensional band-limited functions," *J. Opt. Soc. Am. A* **2** (1985) 693-697.

[10] A. Zakhor; A.V. Oppenheim, "Reconstruction of two-dimensional signals from level crossings," *Proceedings of the IEEE* **78** (1990) 31-55.